

Interpreting LIGO Data Tutorial

SHANNON SCOFIELD¹ AND COLIN MADDEN²

¹Math Department, College of Natural Sciences, University of Texas at Austin, Austin, TX, 78712

²Aerospace Engineering Department, Cockrell School of Engineering, University of Texas at Austin, Austin, TX, 78712

ABSTRACT

The study of gravitational waves is growing and outputting vast amounts of data for study. The largest gravitational wave observatory is the Laser Interferometer Gravitation-Wave Observatory out of California operated by Caltech and MIT. LIGO's data archive at Caltech holds over 4.5 Petabytes of data, and will grow at a rate of about 0.8 Pb per year and processing and analyzing all of LIGO's data requires a vast computing infrastructure. The data released by LIGO is often noisy due to the difficulty of observing gravitational waves, and a method for extracting signal information from this data will be presented in this paper.

Keywords: Gravitational waves (678) — Gravitational wave detectors (676) — Relativistic astrophysics (1393) — LIGO(920)

1. INTRODUCTION

The study of gravitational waves originates from predictions made by Einstein (1918) in his General Theory of Relativity. He theorized that dynamical systems in strong gravitational fields will release large amounts of energy in the form of gravitational radiation. However, there are a few difficulties in the observation of such waves. For example, in the neighborhood of Earth predicted amplitudes or strains in space caused by gravitational waves from astrophysical events are extremely small, and in order to detect such events an amplitude sensitivity close to 10^{-22} is required. In addition, gravitational wave signals are expected over a wide range of frequencies, with signals of frequency 10-17 Hz in the case of small disturbances in the cosmological background, through 103 Hz when neutron stars are born in supernova explosions, up to possible signals in the GHz range from processes in the early Universe. This broad possible range is why the sensitivity above is required over approximately 1000 Hz to detect events just in our vicinity. What does detecting gravitational waves give us? Gravitational radiation carries the signs of the nature of spacetime geometry and therefore is incredibly useful to understand the behavior of matter and geometry under extreme density, temperature, magnetic fields, and relativistic motion. Gravitational wave detection has impacted the verification of theories about how gravity travels, the understanding of black holes, and the verification of a possible multiverse. In addition, the development of the technology required to observe gravitational waves has resulted in advancements several technological areas. For example, the development of ultra-stable oscillators and parametric transducers for gravitational wave detection have led to developments in quantum observation technology. In addition there are developments in space technology, cryogenics, material science, and grid computing attributed to gravitational wave research. (Marx et al. 2011)

2. OBJECTIVE

This tutorial will explain the methods and processes by which noisy gravitational wave signal data from the Laser Interferometer Gravitational-Wave Observatory, or LIGO, is transformed into data that can be investigated and analyzed to obtain further information about the cosmic events that produce these gravitational waves.

3. METHODOLOGY

The first step in analyzing real-world phenomena is to gather data. A signal is typically gathered using many discretely sampled time-series data. The information from a signal is recorded at many different discrete times, often thousands of times per second. This is referred to as the sampling frequency; how many discrete samples of the signal

42 information is taken per second. The sampling frequency of our instruments defines the accuracy of the information
 43 contained in the data. If the signal's frequency is too high relative to the sampling frequency, some information
 44 contained in the signal will be lost. The Nyquist frequency is this upper limit of the signal frequency allowed before
 45 signal information is lost. The Nyquist frequency, f_n , is defined as half of the sampling frequency, f_s .

$$f_n = \frac{f_s}{2} \quad (1)$$

46 For example, consider an instrument with a sampling frequency of 20Hz, or 20 samples per second. The Nyquist
 47 frequency is then 10Hz. Signals which have a frequency of 10Hz or higher will not portray their true information when
 48 viewed through the lens of 20Hz sampling frequency.

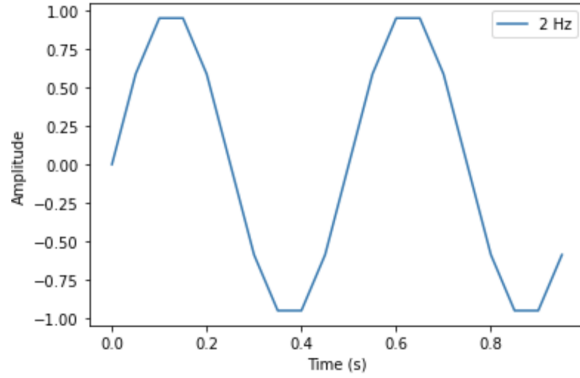


Figure 1. Plot of a 2Hz Sine Wave with 20Hz sampling frequency

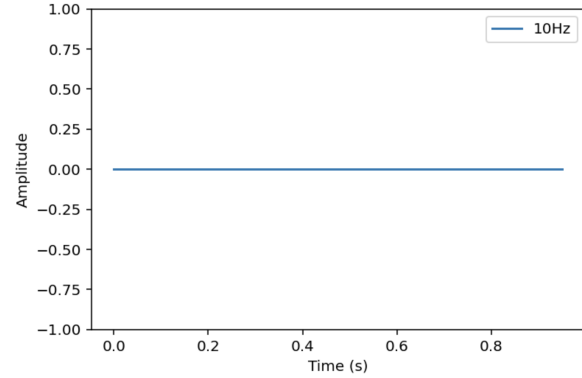


Figure 2. Plot of a 10Hz Sine Wave with 20Hz sampling frequency

50 Figures 1 and 2 show a 2 Hz sine wave and 10 Hz sine wave respectively plotted with a 20 Hz sampling frequency.
 51 As evident in Figure 1, the sine wave for the 2 Hz signal is visible. The peaks and troughs are clear, and the
 52 oscillations are evident. Now for the 10Hz sine wave in Figure 2, it appears to just be a straight line. This is due
 53 to the fact that the frequency of the sine wave is equal to the Nyquist frequency. The entirety of the information of
 54 the 10Hz sine wave is lost. There is no clear information in this data, even though there should be oscillations in the
 55 data. This evinces the importance of a high sampling frequency relative to the signal frequency we are trying to observe.

56 After showcasing the importance of frequency in data, let's take a look at viewing the actual frequencies that are
 57 hidden in signal data. In a real-world signal there is not ever one singular frequency that the data is comprised of.
 58 Instead, the data is comprised of many different frequencies from various factors such as noise and disturbances. To
 59 view the frequencies that make up a signal, the signal must be converted from the time domain to the frequency
 60 domain. This is achieved by using a fast Fourier transform, or FFT. The Fourier transform breaks up data into a
 61 composition of sine and cosine waves with various amplitude and frequencies that can replicate the data. This allows
 62 the observation of dominant frequencies that comprise the data. The formula of the Fourier transform is shown below:

$$\tilde{x}(f) = \int_{-\infty}^{\infty} x(t)e^{-i2\pi ft}dt \quad (2)$$

63 where $x(t)$ is the signal data, e is Euler's number, i is the imaginary unit, f is the frequency, and t is time. The
 64 value of $|\tilde{x}(f)|^2$ is also known as the energy spectral density. The square root of the energy spectral density, $\sqrt{|\tilde{x}(f)|^2}$
 65 is known as the amplitude spectral density, ASD.

66 Figure 3 shows a plot of noisy data in the time domain. There are clear oscillations in the data, but there is no
 67 evident pattern visible to the naked human eye. However, Figure 4 shows this same plot of data but in the frequency
 68 domain. Examining Figure 4 shows a clear picture of what frequencies compose the data. There are 3 sine waves that
 69 combine to create the data in Figure 3. A frequency of 220 Hz is the dominant frequency as evident by the higher
 70 amplitude. The second most dominant frequency is 190 Hz and the third frequency is 310 Hz, seen by the descending
 71 amplitude. The third frequency is the lowest amplitude. The second frequency is the second highest amplitude.
 72

73

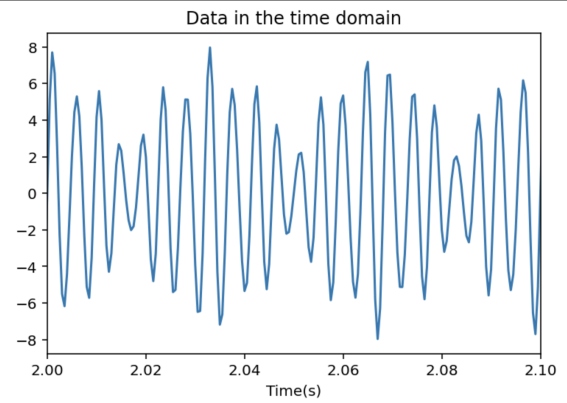


Figure 3. A plot of noisy data in the time domain

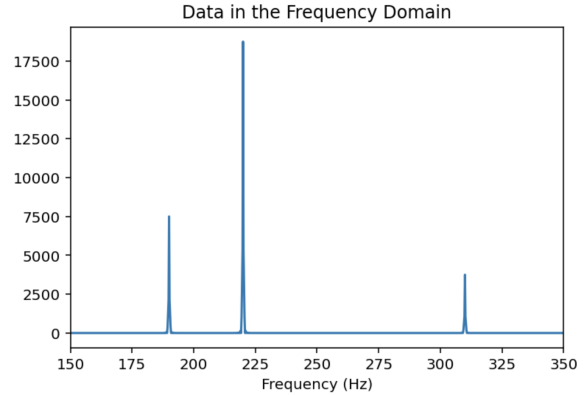


Figure 4. A plot of the same noisy data in the frequency domain

74
75

magnitude of the amplitudes.

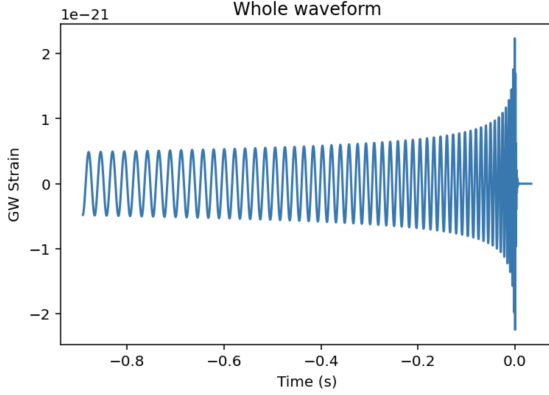


Figure 5. Strain vs time graph of CBC gravitational wave data

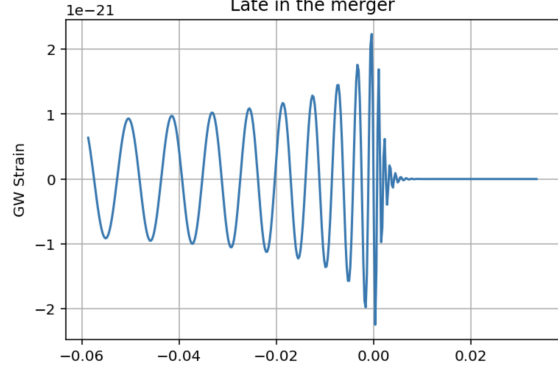


Figure 6. Strain vs time graph of CBC gravitational wave data near the time of merging

76

Now let's apply these techniques to some model gravitational wave data of a compact binary coalescence, or CBC, event. Figure 5 depicts the gravitational wave signal of the merger of two black holes with the mass of 10 solar masses each. The frequency of the waveform evolves with time as the black holes orbit their barycenter. At the beginning of the waveform, the black holes have greater distance between them and as such orbit slower with longer orbital periods. These longer orbital periods result in lower frequency signals. As the orbit of the black holes begins to occur faster, their orbital periods decrease drastically and the frequency near the time of merger increases substantially. In Figure 6, we zoom in on the plot very near the time of the merging. The substantial increase in frequency at the time of merging is highly evident.

84

Now let's view this data in the frequency domain. Figure 7 shows the gravitational wave data in the frequency domain. The signal energy is highest corresponding to our lowest frequencies. This might seem counter-intuitive at first as one will assume that the high frequencies near the time of merging would produce higher energies. However, there is higher signal energy at low frequencies due to the fact that the black holes spend more time orbiting at the frequencies from the slower orbital speed, resulting in more energy. At the higher frequencies there is lower signal energy near the time of the merger because the orbital speed of the black holes is significantly higher. There is a steep drop off in signal energy at the peak frequency, which occurs at the time of merging, as the bodies are reaching their peak orbital velocity.

91

92

What if we want to view this data in both the time and frequency at once? We can do this by utilizing a "Q-transform". A Q-transform utilizes a wavelet basis to transform the data into a representation of the data with both time and frequency. The Q-transform is related to the Fourier transform. Figure 8 depicts this Q-transform of the

93

94

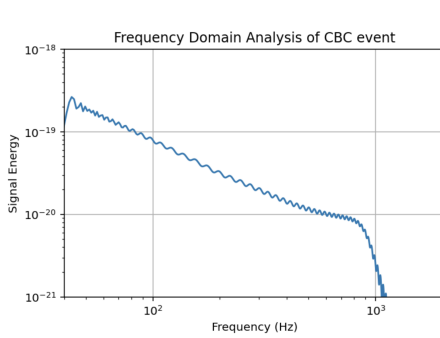


Figure 7. Strain vs time graph of CBC gravitational wave data near the time of merging

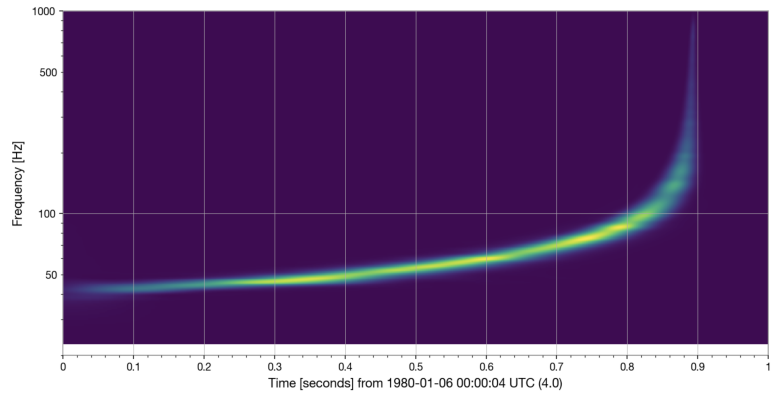


Figure 8. Spectrogram from Q-transform of LIGO data showing both time and frequency

LIGO data in the form of a spectrogram. In the figure, the frequency increases with time as the black holes orbit closer and closer until the time of the merger. Just before the time of merging, the frequency is seen to jump significantly, in line with the data shown in Figures 6 and 7.

Instruments lie. The signal received from an instrument is not always a perfect representation of the data. There is often noise involved in the data processed. Outside noise can result from variety of factors. This signal noise must be processed and considered before any analysis can be undertaken. The sources of noise for LIGO data are plentiful and some are not very well understood. There are 3 main sources of noise we will consider: shot noise, thermal noise, and controls noise. Shot noise dominates the noise pattern for LIGO data at high frequencies. This type of noise results from the uncertainty of the number of photons hitting the photo detector, determined by the Heisenberg uncertainty principle. The second type of noise is thermal noise. Thermal noise is caused by vibrations of molecules on the coating of the mirrors or the wires which hold the mirrors in place. The thermal noise peaks at the frequency of ~ 100 Hz in this case. Controls noise is the third type of noise we will consider. Controls noise consists of a variety of sources at low frequencies. These include seismic noise and radiation pressure noise. We will consider these three sources of noise as our "Cartoon model" of the noise, which excludes some other real world factors which are quite complicated. Figure 9 depicts our Cartoon model of noise vs some noise captured from real data. This shows our model is sufficiently accurate to help us interpret how to process the noise from LIGO data.

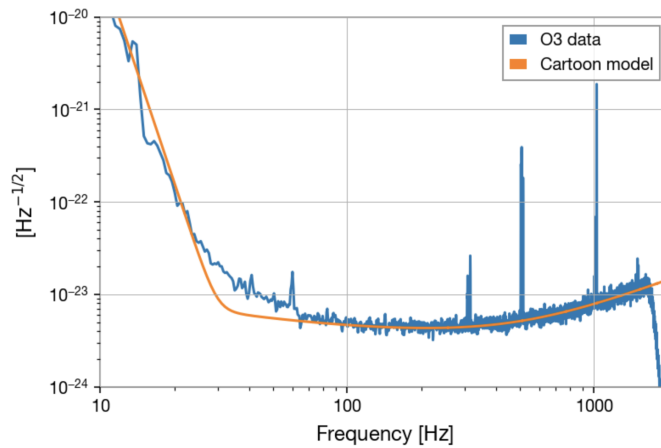


Figure 9. Real-world noise vs Cartoon model of noise

These sources of noise are dependent on frequency. Due to this, some parts of the LIGO signal will be hidden by the noise, most particularly in the low frequencies. Figure 10 shows how the early parts of the signal will be hidden

114 by the noise. The frequency of the signal is only apparent right before the merger when the frequency of the signal is
 115 high enough to overcome the significant noise. This showcases the importance of the processing of noise in data.

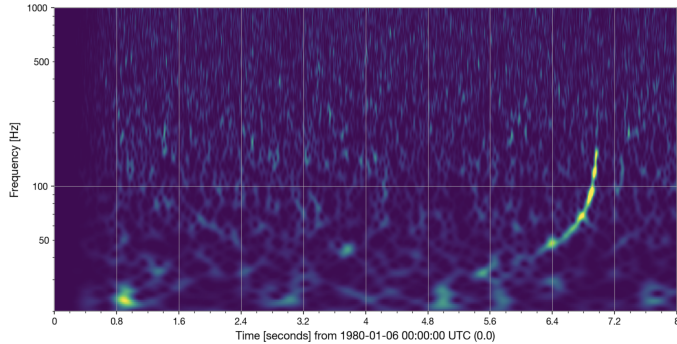


Figure 10. Spectrogram of LIGO data in time and frequency with noise added

116 There are a few basic tools used in signal processing to filter out noise: whitening and band-pass filtering. Let's take
 117 a look of the time domain and frequency domain of raw data. Figure 12 shows raw LIGO data in the time domain
 118 with included noise. Figure 11 shows raw LIGO data in the frequency domain with included noise. In Figure 11, the
 119 amplitude at ~ 6 Hz is about 4 magnitude higher than the frequency at target "bucket" frequency at 100 Hz. This is
 120 the due to the domination of the low frequency noise in the data, seen in Figure 12 as the wiggles in the plot. Applying
 121 the process of whitening, we will smooth the data out so that there are about equal amplitude for all frequencies.
 122 This suppresses areas abundant in noise and accentuates areas low in noise. Figure 13 shows the result of this process.
 123 Band-pass filtering is the secondary process by which noise is processed. Band-passing is the operation that removes
 124 any noise and signals outside of a desired band of frequency. Figures 14 and 15 show the result of band-passing raw
 125 LIGO data in the range of frequencies between 40 and 400 Hz. Only the frequencies between these two values will
 126 passed through the filter and kept. Now, the time domain plot in Figure 15 shows the signal in the center of the plot.
 127 The removal of frequencies outside the desired range is also visible in Figure 14 (Abbott et al. 2020)

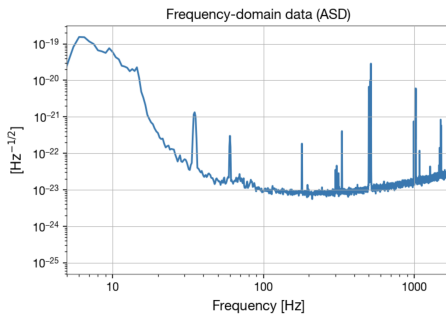


Figure 11. Frequency domain LIGO data with included noise

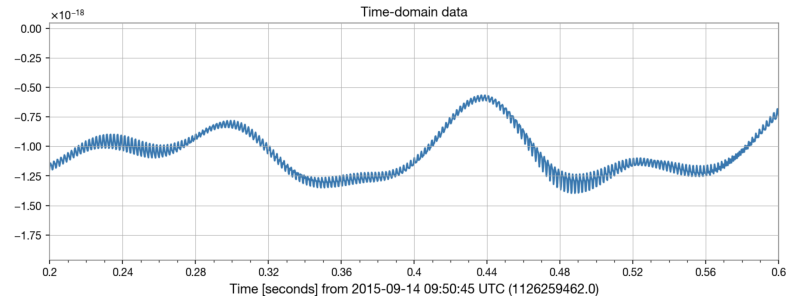


Figure 12. Time domain LIGO data with included noise

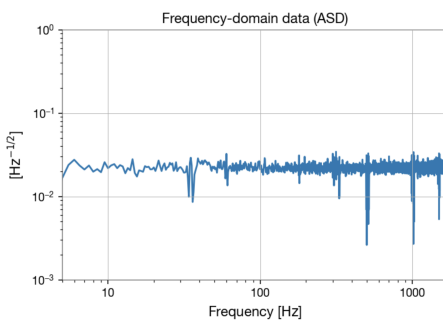


Figure 13. Whitened raw LIGO data

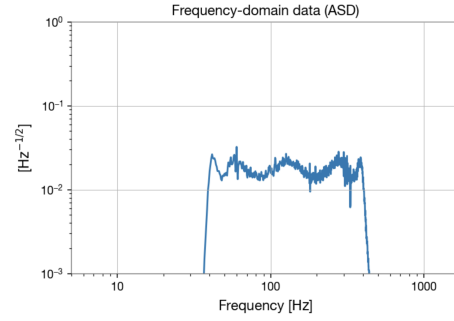


Figure 14. LIGO data in the frequency domain with band-pass filtering 40-400 Hz

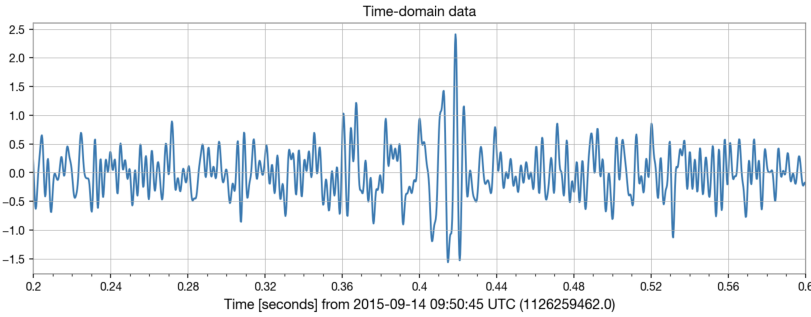


Figure 15. LIGO data in the time domain with band-pass filtering 40-400 Hz

4. CONCLUSION

From the computations performed above, one can find the times of the zero-crossings of the signal and use those to calculate the period (P_{gw}) and frequency (f) of the gravitational wave. Then calculations can be done to compute the chirp mass of a binary system. The chirp mass of a binary system is defined to be:

$$M_c = \frac{(m_1 m_2)^{\frac{3}{5}}}{(m_1 + m_2)^{\frac{1}{5}}} \quad (3)$$

It can also be measured using the time derivative of the frequency of the gravitational wave, \dot{f} , via the equation

$$M_c = \frac{c^3}{G} \left[\left(\frac{5}{96} \right)^3 \pi^{-8} f^{-11} \dot{f}^3 \right]^{\frac{1}{5}} \quad (4)$$

However, this method can run into calculation issues if noise and calculation errors result in a negative \dot{f} . Thus instead the chirp mass can be found from the slope of $f^{-\frac{8}{3}}$.

If you integrate the last expression, the result is:

$$f^{-\frac{8}{3}} = \frac{(8\pi)^{\frac{5}{3}}}{5} \left(\frac{GM_c}{c^3} \right) (t_c - t) \quad (5)$$

where t_c is the time of coalescence. With the data set's time origin as the merger event, $t_c = 0$, when you differentiate this, you will find that the chirp mass, M_c , is proportional to the slope of $f^{-\frac{8}{3}}$:

$$\frac{df^{-\frac{8}{3}}}{dt} = \text{slope} = s = -\frac{(8\pi)^{\frac{5}{3}}}{5} \left(\frac{GM_c}{c^3} \right) \quad (6)$$

Setting the slope as the variable s , the chirp mass is then:

$$M_c = \frac{c^3}{G(8\pi)^{\frac{8}{3}}} (-5s)^{\frac{3}{5}} \quad (7)$$

Using information regarding known binary systems the type of system can be inferred using the calculated chirp mass. If the chirp mass significantly smaller than observed black hole systems, it is likely to be a pair of neutron stars. If it is a pair of neutron stars, an assumption can be made about the mass of one of the objects (m_1) using the Chandrasekhar limit. Then using Equation 3 the roots of the equation can be solved for to obtain m_2 . Then Kepler's Law

$$P_{orb}^2 = R^3 \left[\frac{4\pi^2}{G(m_1 + m_2)} \right] \quad (8)$$

where P_{orb} is the orbital period, and R is the orbital radius (semi-major axis for elliptical orbits), and because the lowest order of gravitational radiation is quadrupolar, the period of a gravitational wave, P_{gw} , is half the orbital period of the system ($P_{orb} = 2P_{gw}$). This equation can be solved for R

$$R = \left[G(m_1 + m_2) \left(\frac{P_{orb}}{2\pi} \right)^2 \right]^{\frac{1}{3}} \quad (9)$$

Using this form of the equation and the fact that $P_{orb} = 2P_{gw}$ the orbital separation in the time before the merger can be calculated like in Figure 16.

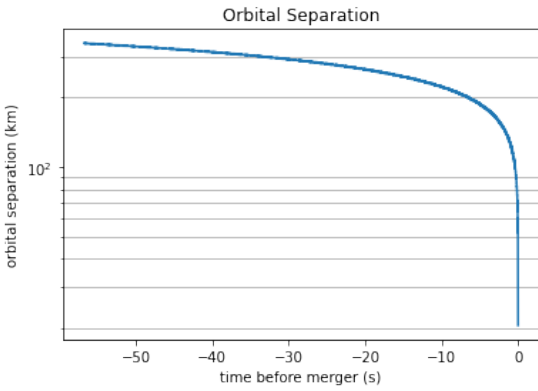


Figure 16. Graph of the orbital separation of the two masses in the time before the merger

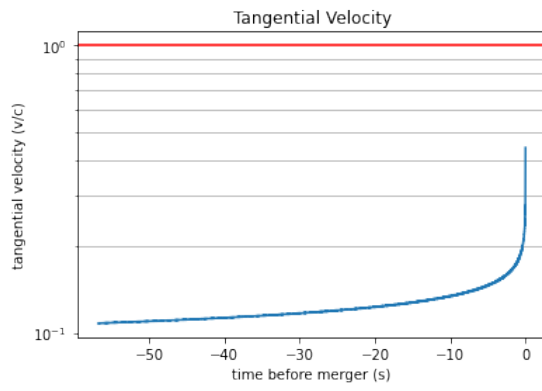


Figure 17. Graph of the tangential velocity of the two masses in the time before the merger

The orbital separation values, when compared to the size of a normal star can inform the analyst about the correctness of the assumption regarding the two masses of the system. In the case above, the largest orbital separation is smaller than the radius of a normal star like that of the Earth's Sun; therefore, it is likely that the system is made up of two neutron stars. Then, given the orbital distance, R , and the orbital period, P_{orb} , calculations can be done to determine the tangential velocity of the binary system during its evolution:

$$v = 2\pi \left(\frac{R}{P_{orb}} \right) \quad (10)$$

An example of this calculation as performed on LIGO data from a binary system can be seen in Figure 17. From this, it can be seen that the linearized approximation of general relativity has its limits because as we approach merger our tangential velocity exceeds the speed of light. Additional information that can be derived from gravitational wave data includes measuring the Hubble constant (Abbott et al. 2021) and inferences regarding the population of binary black holes (Abbott et al. 2019).

REFERENCES

- Abbott, B. P., Abbott, R., Abbott, T. D., et al. 2021, A Gravitational-wave Measurement of the Hubble Constant Following the Second Observing Run of Advanced LIGO and Virgo, doi: [10.3847/1538-4357/abdcbb](https://doi.org/10.3847/1538-4357/abdcbb)
- . 2019, Binary Black Hole Population Properties Inferred from the First and Second Observing Runs of Advanced LIGO and Advanced Virgo, doi: [10.3847/2041-8213/ab3800](https://doi.org/10.3847/2041-8213/ab3800)

- 174 —. 2020, A guide to LIGO–Virgo detector noise and
175 extraction of transient gravitational-wave signals, IOP
176 Publishing, doi: [10.1088/1361-6382/ab685e](https://doi.org/10.1088/1361-6382/ab685e)
- 177 Einstein, A. 1918, Über Gravitationswellen.
178 <https://ui.adsabs.harvard.edu/abs/1918SPA.....154E>
- 179 Marx, J., Danzmann, K., Hough, J., et al. 2011, The
180 Gravitational Wave International Committee Roadmap:
181 The future of gravitational wave astronomy,
182 doi: [10.48550/arXiv.1111.5825](https://arxiv.org/abs/1111.5825)